



OPEN

SUBJECT AREAS:
NANOWIRES
INORGANIC LEDsReceived
17 September 2014Accepted
28 November 2014Published
16 January 2015Correspondence and
requests for materials
should be addressed to
Z.M. (zetian.mi@
mcgill.ca)

Engineering the Carrier Dynamics of InGaN Nanowire White Light-Emitting Diodes by Distributed p -AlGaN Electron Blocking Layers

Hieu Pham Trung Nguyen^{1,2}, Mehrdad Djavid¹, Steffi Y. Woo³, Xianhe Liu¹, Ashfiqua T. Connie¹, Sharif Md. Sadaf¹, Qi Wang¹, Gianluigi A. Botton³, Ishiang Shih¹ & Zetian Mi¹

¹Department of Electrical and Computer Engineering, McGill University, 3480 University Street, Montreal, Quebec H3A 0E9, Canada, ²Department of Electrical and Computer Engineering, New Jersey Institute of Technology, University Heights, Newark, New Jersey 07102, ³Department of Materials Science and Engineering, Canadian Centre for Electron Microscopy and Brockhouse Institute for Materials Research, McMaster University, 1280 Main Street West, Hamilton, Ontario L8S 4L7 Canada.

We report on the demonstration of a new type of axial nanowire LED heterostructures, with the use of self-organized InGaN/AlGaN dot-in-a-wire core-shell nanowire arrays. The large bandgap AlGaN shell is spontaneously formed on the sidewall of the nanowire during the growth of AlGaN barrier of the quantum dot active region. As such, nonradiative surface recombination, that dominates the carrier dynamics of conventional axial nanowire LED structures, can be largely eliminated, leading to significantly increased carrier lifetime from ~ 0.3 ns to 4.5 ns. The luminescence emission is also enhanced by orders of magnitude. Moreover, the p -doped AlGaN barrier layers can function as distributed electron blocking layers (EBLs), which is found to be more effective in reducing electron overflow, compared to the conventional AlGaN EBL. The device displays strong white-light emission, with a color rendering index of ~ 95 . An output power of >5 mW is measured for a $1\text{ mm} \times 1\text{ mm}$ device, which is more than 500 times stronger than the conventional InGaN axial nanowire LEDs without AlGaN distributed EBLs.

Group III-nitride nanowire heterostructures (e.g., InGaN) have been intensively studied as an emerging platform for future solid-state lighting and full-color display. Various axial and radial nanoscale heterostructures, including dot/disk/well-in-a-wire and core-shell nanowires have been developed^{1–12}. To date, InGaN/GaN core-shell radial heterostructures have been commonly grown by metal organic vapour phase epitaxy (MOVPE)^{9,10,13–17}, wherein InGaN/GaN multiple quantum wells can be formed on the nonpolar m -plane sidewalls of GaN nanowires^{13,15–18}. Such core-shell structures exhibit massively enhanced surface emission area and reduced, or even completely eliminated polarization fields. One of the major obstacles for achieving high efficiency full-color LEDs, however, lies in incorporating high In content for deep green and red emission^{14,15}. Moreover, the realization of large area core-shell LEDs is limited by the difficulty in achieving homogeneous current spreading, due to the non-planar fabrication process associated with radial nanowires. As a consequence, most of these studies have been focused on single radial nanowire devices^{1,9,13}. Alternatively, catalyst-free, uniform In(Al)GaN axial nanowire arrays can be formed directly on large area Si substrates by molecular beam epitaxy (MBE)^{2,3,6,19–22}, with the device structure and fabrication process nearly identical to that of commercial planar LED devices. Large area InGaN nanowire LEDs with emission wavelengths in the range of ultraviolet to near-infrared have been demonstrated^{15,14,23–26}. The carrier dynamics of such devices, however, has been adversely affected by the uncontrolled surface recombination, leading to extremely short carrier lifetime (~ 0.3 ns, or less)^{27–29}. The dominance of nonradiative surface recombination has been identified as the major cause for the low quantum efficiency and the very low output power (nW to μ W) of axial nanowire LEDs^{7,26,30}. In this regard, various surface passivation techniques^{27,28,31–33} have been explored, among which the use of an *in situ* grown large bandgap shell has shown to be highly promising and effective in improving the device performance^{27,34–36}. However, the controllable formation of such a uniform shell (e.g. AlGaN) for large scale, catalyst-free InGaN/GaN axial nanowire arrays has been elusive. Moreover, its impact on the carrier dynamics, including the charge carrier lifetime, injection and transport process has remained unknown.

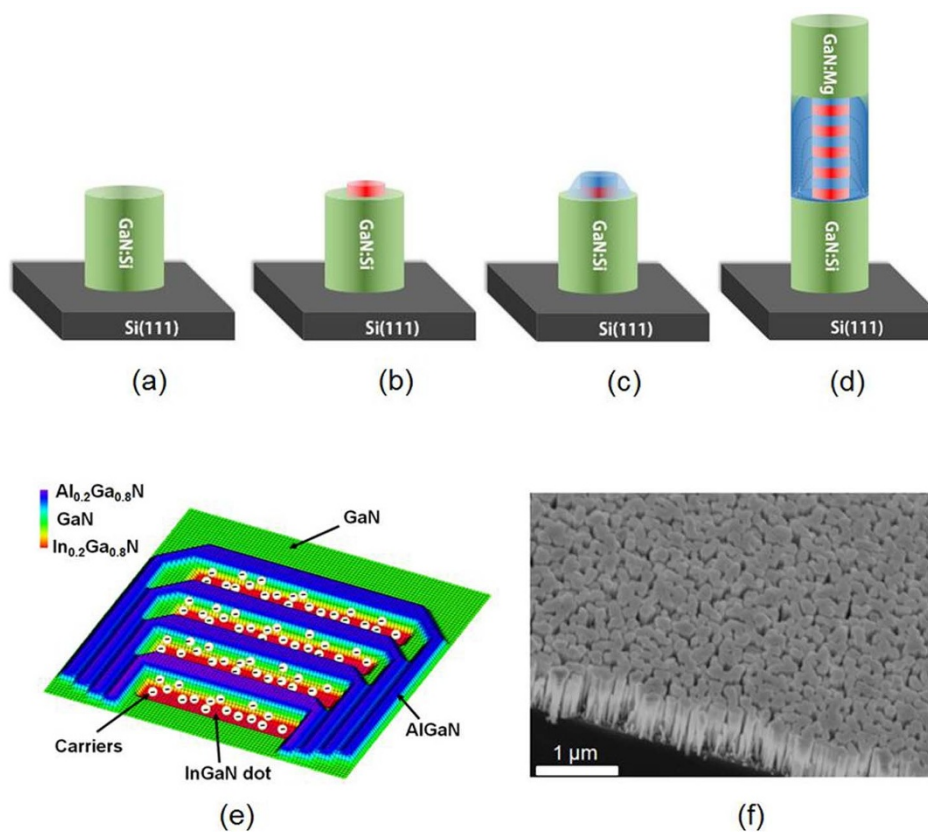


Figure 1 | (a)–(d) Illustration of the epitaxial growth of catalyst-free InGaN/AlGaN dot-in-a-wire core-shell LED heterostructures on Si substrate. (a) GaN:Si segment was first grown on Si(111) substrate. (b) 3 nm InGaN dot was grown on GaN:Si. (c) The formation of AlGaN barrier and shell. (d) The formation of a thick AlGaN shell surrounding the InGaN quantum dot active region after the growth of multiple, vertically aligned InGaN/AlGaN dots. (e) Schematic illustration of the energy band diagram of the InGaN/AlGaN dot-in-a-wire core-shell LED active region, showing the three-dimensional carrier confinement. (f) A 45° tilted SEM image of a typical InGaN/AlGaN dot-in-a-wire core-shell LED heterostructure grown on Si substrate.

In this context, we have developed a new type of LED heterostructures, with the use of self-organized InGaN/AlGaN dot-in-a-wire core-shell nanowire arrays that can address the afore-mentioned critical challenges for achieving large area, high efficiency, full-color LEDs. In this process, during growth of the AlGaN barrier of the quantum dot active region, an AlGaN shell is also spontaneously formed on the sidewall of the nanowire, which can lead to drastically reduced nonradiative surface recombination. By controlling the AlGaN barrier thickness and/or compositions, the carrier lifetime can be effectively varied in the range of ~ 0.3 ns to 4.5 ns, leading to dramatically enhanced carrier injection efficiency and light output. Also unique to this core-shell structure is that the AlGaN barrier layers can function as distributed EBLs, which is found to be much more effective in reducing electron overflow, one of the primary causes of efficiency droop, compared to the conventional AlGaN EBL. Moreover, the hole injection and transport process can be significantly enhanced in such InGaN/AlGaN quantum dot superlattice structures. The device exhibits strong white light emission, due to compositional variations of the dots. An output power of more than 5 mW is measured for an InGaN/AlGaN dot-in-a-wire LED device, with an unprecedentedly high color rendering index of ~ 95 .

Catalyst-free InGaN/AlGaN dot-in-a-wire core-shell nanowire LED heterostructures were grown on Si substrates by radio-frequency plasma-assisted MBE (see Methods). The self-organized formation process of the dot-in-a-wire core-shell heterostructures is schematically illustrated in Figures 1(a)–(d). GaN:Si nanowires, with a height of 0.4 μm , were first grown directly on Si substrate. Shown in Figure 1(b), the InGaN dot, with a height of ~ 3 nm is formed at the center of the nanowire. Due to the strain-induced

self-organization, the dot diameter is smaller than the nanowire dimension. The subsequently grown AlGaN barrier layer can cover the entire growth front, including the top and sidewalls of the InGaN dot, illustrated in Figure 1(c), thereby leading to the spontaneous formation of a large bandgap shell structure. The repeated growth of multiple, vertically aligned InGaN/AlGaN quantum dots, shown in Figure 1(d), enable the formation of a relatively thick, uniform AlGaN shell surrounding the device active region. The barrier of each quantum dot is also modulation doped *p*-type using Mg to enhance hole transport^{7,37}. White light emission with well controlled properties can be achieved by varying the In compositions of the dots. Finally, a 0.2 μm GaN:Mg section was grown on top, shown in Figure 1(d). Figure 1(e) shows the energy band diagram of the InGaN/AlGaN dot-in-a-wire core-shell LED active region, which exhibits superior three-dimensional carrier confinement, due to the multiple AlGaN shell and barrier layers.

Figure 1(f) is a 45 degree-tilted scanning electron microscopy (SEM) image for an InGaN/AlGaN dot-in-a-wire core-shell heterostructure grown on Si(111) substrate. It is seen that the vertically aligned nanowire arrays exhibit a high degree of size uniformity. Previous studies have shown that the majority of nanowires grown on Si by MBE are N-polar^{38,39}. In order to examine the effect of AlGaN shell on the performance of nanowire LEDs, several InGaN/AlGaN nanowire samples with different Al compositions in the barrier layers were grown. LED 1, LED 2, LED 3, and LED 4 correspond to Al beam equivalent pressures (BEP) of 8.27×10^{-9} , 1.52×10^{-8} , 2.42×10^{-8} , and 3.84×10^{-8} Torr, respectively. An InGaN/GaN dot-in-a-wire LED structure was also grown for comparison.

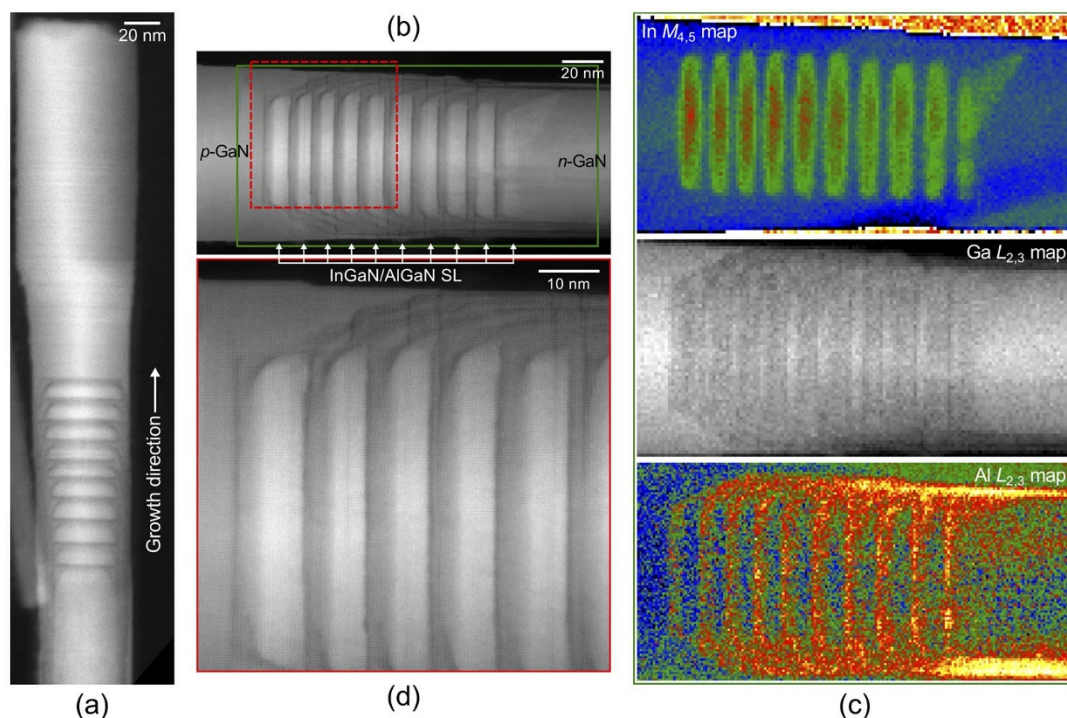


Figure 2 | (a, b) STEM-HAADF images of the InGaN/AlGaN dot-in-a-wire core-shell heterostructures showing the InGaN dots, AlGaN barriers, and the Al-rich core-shell by atomic-number contrast. The acquisition area of the EELS spectrum image is boxed in green in (b). (c) Elemental mapping from EELS spectrum imaging of the green area marked in (b) of the group III elements extracted from the In $M_{4,5}$, Ga $L_{2,3}$, and Al $L_{2,3}$ -edges. (d) Higher magnification atomic-resolution HAADF image of the selected region (boxed in red dashed line) in (b) showing the AlGaN core-shell and barriers in detail.

High-angle annular dark-field (HAADF) atomic-number contrast imaging of single nanowires is shown in Figures 2(a) and (b), presenting clearly the ten InGaN/AlGaN quantum dots in the GaN nanowire. A detailed view of the active region in Figure 2(b) shows that the ten InGaN dots (bright contrast) are centrally confined and capped by the AlGaN barriers (dark contrast), each of which form an Al-rich core-shell at the nanowire sidewall. Elemental analysis was performed using electron energy-loss spectroscopy (EELS) in scanning transmission electron microscope (STEM) on the nanowire in Figure 2(b). Elemental maps from spectrum imaging in Figure 2(c) illustrate the distribution variation of group III elements in the different regions. The In-map extracted from the In $M_{4,5}$ -edge shows a strong localization in only the quantum dots. The Ga-map shows a signal maximum towards the center of the nanowire because of the increased projected thickness, as well as an overall deficiency in the active region and at the sidewalls in the presence of In or Al alloying elements. Most notable is the Al distribution in the AlGaN barrier layers and the Al-rich core-shell in the Al-map extracted with the Al $L_{2,3}$ -edge. The Al-rich core-shell is continuous from each of the AlGaN barriers and is present throughout the whole active region and propagates well into the n -GaN segment (also visible in Figure 2(a)). A higher magnification HAADF image of the core-shell in the $\langle 11\bar{2}0 \rangle$ orientation (Figure 2(d)) also shows the continuity of the core-shell from the AlGaN barriers, suggesting their formation during the growth of the AlGaN barriers from the strong lateral diffusion of Al-rich AlGaN. The overall high crystalline quality of the dot-in-a-wire core-shell heterostructures is demonstrated in the atomic-resolution images of Figures 2(b) and (d).

Results

Enhanced photoluminescence (PL) intensity. Photoluminescence spectra of nanowire LED structures were measured using a 266 nm

diode-pumped solid-state laser as the excitation source at room-temperature. The PL emission was spectrally resolved by a high-resolution spectrometer, and detected by a photomultiplier tube. Figure 3(a) shows the PL spectra of an InGaN/AlGaN core-shell nanowire LED (LED 3, solid blue) and an InGaN/GaN dot-in-a-wire structure with otherwise identical conditions (dotted black). The PL emission results primarily from localized exciton recombination in InGaN and exhibits broad spectral linewidth, due to In alloy fluctuations^{40,41}. It is seen that the core-shell LED structure exhibits significantly enhanced PL intensity for emission from InGaN quantum dots (peak wavelength at ~ 550 nm), which is a factor of ~ 10 times higher than that of InGaN/GaN nanowire LEDs without using any AlGaN shell. The enhancement in PL intensity is directly correlated with the increase of Al composition in the AlGaN barrier layers (see Supporting Information, Figure S1). This is explained by the drastically reduced nonradiative surface recombination, due to the presence of large bandgap AlGaN shell, that leads to much more efficient carrier injection and radiative recombination in the quantum dot active region⁴². Interestingly, significantly enhanced PL emission is also observed from GaN (peak wavelength at ~ 364 nm) in these nanowire structures, due to the formation of an AlGaN shell surrounding the n -GaN segment (see Figures 2(a) and (c)), which dominates the emission of GaN. Additionally, the significantly enhanced PL intensity of the InGaN/AlGaN core-shell LED heterostructures can be further confirmed when only the quantum dots are excited by a 405 nm laser (see Supporting Information, Figure S2).

Improved carrier lifetime. We have further conducted time-resolved PL measurements to investigate the impact of AlGaN shell structure on the carrier dynamics of nanowire LED structures. The measurements were performed using a Horiba *DynaMyc* system equipped with a time-correlated single photon

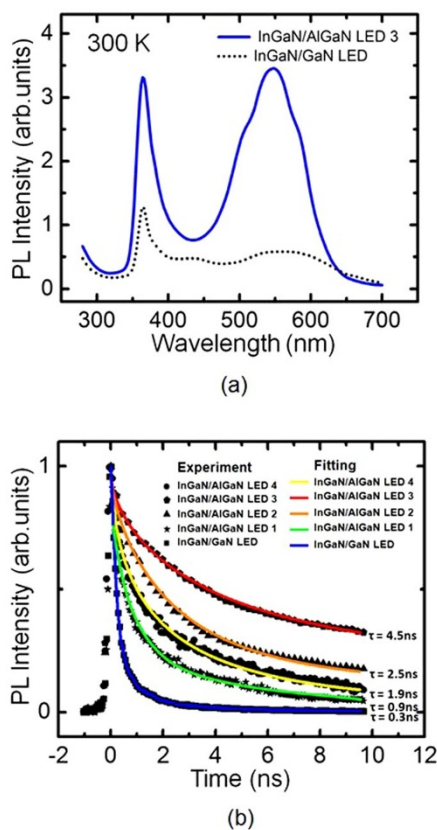


Figure 3 | (a) Photoluminescence spectra showing significantly enhanced emission for the InGaN/AlGaN dot-in-a-wire core-shell LED structure, compared to the InGaN/GaN nanowire sample without AlGaN shell. (b) Time-resolved photoluminescence emission of InGaN/AlGaN dot-in-a-wire core-shell and InGaN/GaN nanowire LED heterostructures, showing the impact of AlGaN shell on the carrier lifetime.

counting (TCSPC) system. A pulsed 375 nm diode laser with a 100 MHz repetition rate was used as the excitation source, and the laser beam was focused on the sample through a 50 \times objective lens. The signal was detected by a TBX picosecond detection module after a long pass filter (>400 nm). Illustrated in Figure 3(b), variations of the PL intensity vs. time can be well described by a standard stretched exponential model,

$$I(t) = I(0)e^{-\left(\frac{t}{\tau}\right)^\beta} \quad (1)$$

where $I(t)$ denotes the time-varying PL intensity, τ is the lifetime, and β is the stretching parameter⁴³. This suggests that the carrier dynamics of InGaN/AlGaN dot-in-a-wire core-shell structures resemble, to a large extent, to that of a heavily disordered system, due to the presence of In-rich nanoclusters^{44–47}. It is seen that the derived carrier lifetime increases dramatically with Al composition,

listed in Table I. For a typical InGaN/GaN axial nanowire LED sample, the carrier lifetime is ~ 0.3 ns^{27–29}. However, with increasing Al incorporation in the AlGaN barrier layer, the carrier lifetime increases to ~ 0.9 , 2.5, and 4.5 ns for LED 1, LED 2, and LED 3, respectively. Since all the samples exhibit nearly identical PL spectra (see Supporting Information, Figures S1 and S2) and are grown under similar conditions, the significantly increased carrier lifetime is attributed to the reduced nonradiative surface recombination⁴³, due to the effective lateral confinement offered by the large bandgap AlGaN shell (see Figure 2). The carrier lifetime of LED 3 is comparable to that of high performance GaN-based quantum well LED structures with emission in the blue/green spectral range^{43,48,49}. Given its direct correlation with the significantly enhanced PL intensity of the InGaN/AlGaN core-shell nanowire LED samples (see Figure 3(a)), we can rule out the quantum-confined Stark effect as the major cause for the increased carrier lifetime. It is also noticed that LED 4 has a shorter carrier lifetime, compared to LED 2 and LED 3, despite of the increased Al composition. This is possibly related to the increased strain and defects in the active region, resulted from the higher Al compositions. It is also worthwhile mentioning that the carrier dynamics is further influenced by the carrier transfer between In-rich nanoclusters^{45,50}, which was not considered in the analysis above. For the best performance InGaN/AlGaN core-shell LEDs (LED 3), the optimum Al composition in the AlGaN barrier is estimated to be in range of 15% to 20%. Further improving the carrier lifetime will involve the optimization of the uniformity of AlGaN shell as well as the Al composition and AlGaN thickness.

Device performance. Such vertically aligned dot-in-a-wire core-shell structures are also compatible with the conventional fabrication process for large area nanowire LED devices (see Methods)^{7,51}. The performance of InGaN/AlGaN core-shell LED devices (LED 3) with an areal size of 1 mm \times 1 mm is described. To minimize junction heating effect, the devices were measured under pulsed biasing conditions ($\sim 1\%$ duty cycle). The InGaN/AlGaN LEDs exhibit excellent current-voltage characteristic with low resistance, shown in Figure 4(a). The output spectra under various injection currents are shown in Figure 4(b). It is seen that the spectra are highly stable and nearly independent of injection currents. The stable emission characteristics with increasing current are further illustrated in the CIE diagram in Figure 4(c). The derived x and y values are in the ranges of ~ 0.35 – 0.36 and 0.37 – 0.38 , respectively. The devices exhibit nearly neutral white light emission, with correlated color temperature of $\sim 4,450$ K and a very large color rendering index of 95. The stable emission is attributed to the large inhomogeneous broadening of the dots and the enhanced hole transport in the p -type modulation doped InGaN/AlGaN quantum dot superlattices.

Illustrated in Figure 4(d), the output power increases monotonically with current. An output power of ~ 5.2 mW and 3.8 mW were measured for LED 3 and LED 2 at an injection current of ~ 600 mA at 10 $^\circ$ C, respectively. Such output powers are more than two orders of magnitude higher than conventional InGaN/GaN axial nanowire

Table 1 | Summary of carrier lifetime measured for InGaN/AlGaN dot-in-a-wire core-shell nanowire LEDs and an InGaN/GaN dot-in-a-wire LED without AlGaN shell

Samples	Al BEP (Torr)	Lifetime (ns)	Stretched parameter, β
InGaN/AlGaN LED 1	8.27×10^{-9}	0.9	0.61
InGaN/AlGaN LED 2	1.52×10^{-8}	2.5	0.55
InGaN/AlGaN LED 3	2.42×10^{-8}	4.5	0.68
InGaN/AlGaN LED 4	3.84×10^{-8}	1.9	0.58
InGaN/GaN LED	0	0.3	0.53
InGaN QW blue LED ^{43,49}	N/A	~ 3.0 – 6.0	N/A
InGaN QW green LED ⁴⁹	N/A	6.2	N/A

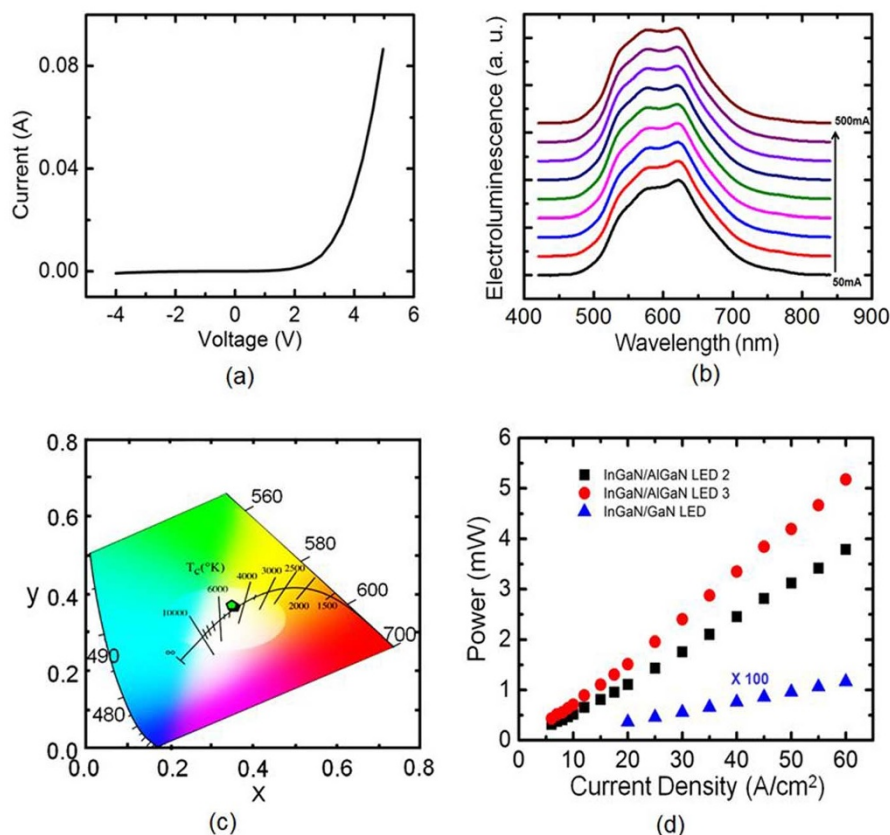


Figure 4 | (a) Current vs. voltage characteristics of an InGaN/AlGaN dot-in-a-wire core-shell white LED on Si. (b) Electroluminescence spectra of LED 3 measured under different injection currents. (c) CIE diagram showing the stable white light emission for injection current from 50 mA to 500 mA, with the x and y values in the ranges of ~ 0.35 – 0.36 and 0.37 – 0.38 , respectively. (d) Output power vs. injection current of the InGaN/AlGaN dot-in-a-wire core-shell LEDs, including LED 2 (black square) and LED 3 (red dot) measured under 1% duty cycle. Variations of the output power vs. current for the InGaN/GaN axial nanowire LED without AlGaN shell are also shown for comparison (blue triangle).

LEDs without AlGaN shell and also much higher than the previously reported InGaN/GaN/AlGaN nanowire LEDs²⁷. The greatly improved output power is attributed to the increased carrier injection efficiency into the device active region, due to the effective carrier confinement offered by the shell structure and the drastically reduced surface recombination⁴². Detailed studies on the device external quantum efficiency further suggest that the nonradiative recombination coefficient is $\sim 1 \times 10^7 \text{ s}^{-1}$ at room-temperature (see Supporting Information, Figure S3), which is significantly smaller than the previously reported values of InGaN/GaN axial nanowire LEDs without using any AlGaN shell⁵². This result is also consistent with the PL and carrier lifetime analysis and further confirms the extraordinary benefits offered by the distributed p -AlGaN EBLs. The measured output power of such unpackaged nanowire LEDs is on the same order of magnitude of previously reported GaN quantum well LEDs⁵³ and can be significantly improved by removing the underlying substrate⁵⁴ and optimizing the light extraction efficiency.

Discussion

In addition to the suppressed nonradiative surface recombination, the effect of InGaN/AlGaN superlattices on the charge carrier transport of nanowire LEDs is further studied using advanced LED device simulation APSYS software. Simulation was performed on InGaN/AlGaN and InGaN/GaN LED heterostructures, as well as an InGaN/GaN structure with the incorporation an equivalent EBL ($\sim 30 \text{ nm}$ thick) (see Supporting Information, Figure S4). An average In composition of $\sim 20\%$ in the dots and 20% Al composition in AlGaN barriers and EBL layer are used in this simulation. Illustrated in Figure 5(a), electron overflow is near-completely suppressed with

the use of InGaN/AlGaN superlattices, which is significantly better than InGaN/GaN LEDs. For comparison, in the conventional EBL design, the use of a relatively thick AlGaN EBL layer adversely affects hole transport from p -GaN to the active region^{55,56}, which leads to non-negligible electron leakage, shown in Figure 5(a). Our studies further confirm that the distributed AlGaN EBL is comparable to, or better than conventional EBL with optimum designs in reducing electron overflow. Moreover, it is evident from Figure 5(a) that, in InGaN/AlGaN dot-in-a-wire core-shell LEDs, the p -AlGaN distributed EBLs can serve as multiple barriers and enable tunnel injection of electrons, thereby leading to significantly reduced hot carrier effect and more uniform carrier distribution across the device active region⁵⁷ (see Supporting Information, Figure S5).

The improved performance by using distributed p -AlGaN EBLs is also directly related to the enhanced hole injection and transport process in the device active region. When InGaN is formed on N -polar AlGaN, the strong internal electric fields, caused by the large differences of the polarizations between the two layers, pull down the bands at the hetero-interface. As a consequence, the acceptor ionization is significantly enhanced. Similarly, the bands are pulled up at the opposite hetero-interface, thereby leading to the formation of two-dimensional hole gas (2DHG)⁵⁸. Previous studies have further shown that the technique of modulation doping, as described above, can drastically increase the hole density for short-period superlattices^{58,59}. Consequently, the hole injection and transport process in the presented InGaN/AlGaN dot-in-a-wire core-shell LED active region can be significantly enhanced. Illustrated in Figure 5(b), detailed simulation further shows that the InGaN/AlGaN LEDs can exhibit enhanced and more uniform radiative recombination,

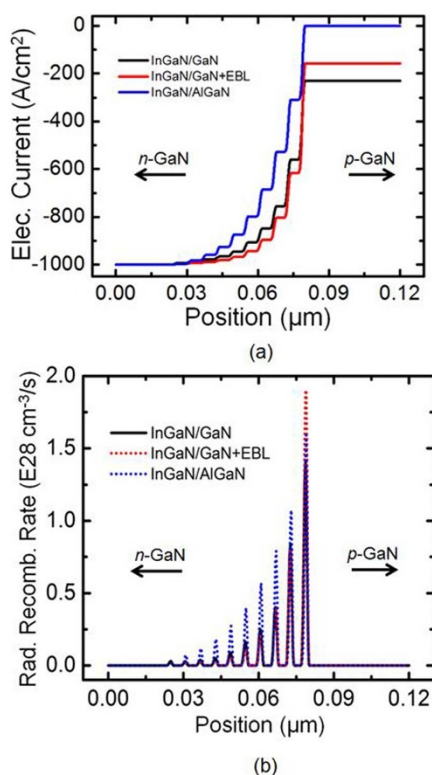


Figure 5 | (a) Simulated electron current density for the InGaN/AlGaN LED (blue), the InGaN/GaN LED with an equivalent electron blocking layer (EBL) (red), and the InGaN/GaN LED (black). (b) Simulated radiative recombination coefficients of the InGaN/AlGaN LED (dotted blue), the InGaN/GaN LED with an EBL (dotted red), and the InGaN/GaN LED (solid black) at an injection current of 1000 A/cm².

compared to InGaN/GaN LEDs, which leads to significantly enhanced output power and reduced efficiency droop (see Supporting Information, Figure S5(c)).

In summary, we have shown that self-organized InGaN/AlGaN dot-in-a-wire core-shell structures can overcome some of the critical challenges of previously reported axial nanowire LEDs, including large surface recombination and poor carrier dynamics, leading to significantly reduced carrier leakage and enhanced output power. Moreover, the *p*-AlGaN barrier layers can function as distributed EBLs, which is found to be highly effective in reducing electron overflow and enhancing hole transport. The dot-in-a-wire core-shell heterostructures can also emit light across the entire visible spectral range and are fully compatible with the conventional planar fabrication process for large area devices. Such unique nanowire heterostructures, with controllable carrier dynamics, will significantly advance the development of a broad range of nanowire photonic devices, including lasers, solar cells, and photodetectors.

Methods

Molecular beam epitaxial growth. In this study, catalyst-free, vertically aligned InGaN/AlGaN dot-in-a-wire core-shell heterostructures were grown on 2 inch *n*-Si(111) substrates by Veeco Gen II MBE system equipped with a radio frequency plasma-assisted nitrogen source under nitrogen rich conditions. Prior to the LED growth, the oxide on the Si surface was removed by hydrofluoric acid (10%) and further thermally *in situ* cleaned at ~770°C. During the growth process, the nitrogen flow rate was kept at 1.0 standard cubic centimeter per minute (sccm), with a forward plasma power of ~350 W. The GaN:Si and GaN:Mg segments were grown at ~770°C. During the growth of the quantum dot active region, the substrate temperature was reduced to 640°C–660°C to enhance In incorporation in the dots. The thickness and Al content of the AlGaN shell can be controlled by the growth duration and Al/Ga flux ratio, respectively.

Structural characterization. A scanning electron microscopy, Hitachi S-4700 system, was used to study the morphology and surface properties of nanowire LED samples. The measurements were performed with a 45-degree angle. An accelerating voltage of 5 kV and a current of 10 μA were used for imaging. Structural properties of InGaN/AlGaN dot-in-a-wire core-shell heterostructures were further performed using a double aberration-corrected Titan³ 80–300 scanning transmission electron microscope.

Device fabrication. The nanowire LEDs were fabricated using the following process. The InGaN/AlGaN dot-in-a-wire core-shell arrays were first spin-coated with polyimide resist for planarization and passivation. Polyimide resist was then etched by O₂ dry etching to reveal the top region of the nanowires. A nearly transparent metal contact including Ni(5 nm)/Au(5 nm)/indium tin oxide (ITO) was deposited on the top GaN:Mg surface of nanowires. Ni/Au metal grid patterns were then deposited on the top of ITO to facilitate current spreading. Ti/Au layers were deposited on the backside of the Si substrate to form *n*-metal contact. The fabricated devices with Ni/Au and Ti/Au metal contacts were annealed at ~500°C for 1 minute in nitrogen ambient.

1. Qian, F. *et al.* Gallium nitride-based nanowire radial heterostructures for nanophotonics. *Nano Lett.* **4**, 1975–1979 (2004).
2. Guo, W., Zhang, M., Banerjee, A. & Bhattacharya, P. Catalyst-free InGaN/GaN nanowire light emitting diodes grown on (001)silicon by molecular beam epitaxy. *Nano Lett.* **10**, 3355–3359 (2010).
3. Kikuchi, A., Kawai, M., Tada, M. & Kishino, K. InGaN/GaN multiple quantum disk nanocolumn light-emitting diodes grown on (111)Si substrate. *Jpn. J. Appl. Phys.* **43**, L1524–L1526 (2004).
4. Kim, H.-M. *et al.* High-brightness light emitting diodes using dislocation-free indium gallium nitride/gallium nitride multiquantum-well nanorod arrays. *Nano Lett.* **4**, 1059–1062 (2004).
5. Guo, W., Banerjee, A., Bhattacharya, P. & Ooi, B. S. InGaN/GaN disk-in-nanowire white light emitting diodes on (001) silicon. *Appl. Phys. Lett.* **98**, 193102 (2011).
6. Lin, H. W., Lu, Y. J., Chen, H. Y., Lee, H. M. & Gwo, S. InGaN/GaN nanorod array white light-emitting diode. *Appl. Phys. Lett.* **97**, 073101 (2010).
7. Nguyen, H. P. T. *et al.* p-Type modulation doped InGaN/GaN dot-in-a-wire white-light-emitting diodes monolithically grown on Si(111). *Nano Lett.* **11**, 1919–1924 (2011).
8. Lauhon, L. J., Gudiksen, M. S., Wang, D. & Lieber, C. M. Epitaxial core-shell and core-multishell nanowire heterostructures. *Nature* **420**, 57–61 (2002).
9. Ra, Y.-H., Navamathavan, R., Yoo, H.-I. & Lee, C.-R. Single nanowire light-emitting diodes using uniaxial and coaxial InGaN/GaN multiple quantum wells synthesized by metalorganic chemical vapor deposition. *Nano Lett.* **14**, 1537–1545 (2014).
10. Koester, R. *et al.* m-Plane core-shell InGaN/GaN multiple-quantum-wells on GaN wires for electroluminescent devices. *Nano Lett.* **11**, 4839–4845 (2011).
11. Li, Q. *et al.* Optical performance of top-down fabricated InGaN/GaN nanorod light emitting diode arrays. *Opt. Express* **19**, 25528–25534 (2011).
12. Liu, B., Smith, R., Bai, J., Gong, Y. & Wang, T. Great emission enhancement and excitonic recombination dynamics of InGaN/GaN nanorod structures. *Appl. Phys. Lett.* **103**, 101108 (2013).
13. Tchernycheva, M. *et al.* InGaN/GaN core-shell single nanowire light emitting diodes with graphene-based p-contact. *Nano Lett.* **14**, 2456–2465 (2014).
14. Qian, F., Gradečák, S., Li, Y., Wen, C.-Y. & Lieber, C. M. Core/multishell nanowire heterostructures as multicolor, high-efficiency light-emitting diodes. *Nano Lett.* **5**, 2287–2291 (2005).
15. Hong, Y. J. *et al.* Visible-color-tunable light-emitting diodes. *Adv. Mater.* **23**, 3284–3288 (2011).
16. Wang, X. *et al.* Continuous-flow MOVPE of Ga-polar GaN column arrays and core-shell LED structures. *Cryst. Growth Des.* **13**, 3475–3480 (2013).
17. Yeh, T.-W. *et al.* InGaN/GaN multiple quantum wells grown on nonpolar facets of vertical GaN nanorod arrays. *Nano Lett.* **12**, 3257–3262 (2012).
18. Liao, C.-H. *et al.* Cross-sectional sizes and emission wavelengths of regularly patterned GaN and core-shell InGaN/GaN quantum-well nanorod arrays. *J. Appl. Phys.* **113**, 054315 (2013).
19. Nguyen, H. P. T., Cui, K., Zhang, S., Fatholouloumi, S. & Mi, Z. Full-color InGaN/GaN dot-in-a-wire light emitting diodes on silicon. *Nanotechnology* **22**, 445202 (2011).
20. Carnevale, S. D. *et al.* Polarization-induced pn diodes in wide-band-gap nanowires with ultraviolet electroluminescence. *Nano Lett.* **12**, 915–920 (2012).
21. Tourbot, G. *et al.* Structural and optical properties of InGaN/GaN nanowire heterostructures grown by PA-MBE. *Nanotechnology* **22**, 075601 (2011).
22. Albert, S. *et al.* Selective area growth of In(Ga)N/GaN nanocolumns by molecular beam epitaxy on GaN-buffered Si(111): from ultraviolet to infrared emission. *Nanotechnology* **24**, 175303 (2013).
23. Wang, Q. *et al.* Highly efficient, spectrally pure 340 nm ultraviolet emission from Al_xGa_{1-x}N nanowire based light emitting diodes. *Nanotechnology* **24**, 345201 (2013).
24. Nguyen, H. P. T. *et al.* High-efficiency InGaN/GaN dot-in-a-wire red light-emitting diodes. *IEEE Photonics Technol. Lett.* **24**, 321–323 (2012).
25. Kishino, K., Kamimura, J. & Kamiyama, K. Near-infrared InGaN nanocolumn light-emitting diodes operated at 1.46 μm. *Appl. Phys. Express* **5**, 031001 (2012).



26. Bavencove, A.-L. *et al.* Submicrometre resolved optical characterization of green nanowire-based light emitting diodes. *Nanotechnology* **22**, 345705 (2011).
27. Nguyen, H. P. T. *et al.* Breaking the carrier injection bottleneck of phosphor-free nanowire white light-emitting diodes. *Nano Lett.* **13**, 5437–5442 (2013).
28. Jahangir, S., Mandl, M., Strassburg, M. & Bhattacharya, P. Molecular beam epitaxial growth and optical properties of red-emitting ($\lambda = 650$ nm) InGaN/GaN disks-in-nanowires on silicon. *Appl. Phys. Lett.* **102**, 071101 (2013).
29. Ebaid, M. *et al.* Ultrashort carrier lifetime of vapor–liquid–solid-grown GaN/InGaN multi-quantum-well coaxial nanorods. *Acta. Mater.* **65**, 118–124 (2014).
30. Choi, J. H. *et al.* Nearly single-crystalline GaN light-emitting diodes on amorphous glass substrates. *Nat. Photon.* **5**, 763–769 (2011).
31. Chevtchenko, S. A. *et al.* Study of SiN_x and SiO₂ passivation of GaN surfaces. *J. Appl. Phys.* **101**, 113709–113707 (2007).
32. Martinez, G. L., Curiel, M. R., Skromme, B. J. & Molnar, R. J. Surface recombination and sulfide passivation of GaN. *J. Electron. Mater.* **29**, 325–331 (2000).
33. Tajik, N., Peng, Z., Kuyanov, P. & LaPierre, R. R. Sulfur passivation and contact methods for GaAs nanowire solar cells. *Nanotechnology* **22**, 7 (2011).
34. Demichel, O., Heiss, M., Bleuse, J., Mariette, H. & Fontcuberta i Morral, A. Impact of surfaces on the optical properties of GaAs nanowires. *Appl. Phys. Lett.* **97**, 201907 (2010).
35. Parkinson, P. *et al.* Carrier lifetime and mobility enhancement in nearly defect-free core–shell nanowires measured using time-resolved terahertz spectroscopy. *Nano Lett.* **9**, 3349–3353 (2009).
36. Scofield, A. C. *et al.* Composite axial/core-shell nanopillar light-emitting diodes at 1.3 μm . *Appl. Phys. Lett.* **101**, 053111 (2012).
37. Xie, J. Q. *et al.* On the efficiency droop in InGaN multiple quantum well blue light emitting diodes and its reduction with p-doped quantum well barriers. *Appl. Phys. Lett.* **93**, 121107 (2008).
38. Fernández-Garrido, S. *et al.* Spontaneous nucleation and growth of GaN nanowires: The fundamental role of crystal polarity. *Nano Lett.* **12**, 6119–6125 (2012).
39. Hestroffer, K., Leclere, C., Bougerol, C., Renevier, H. & Daudin, B. Polarity of GaN nanowires grown by plasma-assisted molecular beam epitaxy on Si(111). *Phys. Rev. B* **84**, 245302 (2011).
40. Chang, Y. L., Wang, J. L., Li, F. & Mi, Z. High efficiency green, yellow, and amber emission from InGaN/GaN dot-in-a-wire heterostructures on Si(111). *Appl. Phys. Lett.* **96**, 013106 (2010).
41. Smith, M. *et al.* Time-resolved photoluminescence studies of InGaN epilayers. *Appl. Phys. Lett.* **69**, 2837–2839 (1996).
42. Shaofei, Z. *et al.* On the carrier injection efficiency and thermal property of InGaN/GaN axial nanowire light emitting diodes. *IEEE J. Quantum Electron.* **50**, 483–490 (2014).
43. Pophristic, M., Long, F. H., Tran, C., Ferguson, I. T. & Karlicek, R. F. Time-resolved photoluminescence measurements of InGaN light-emitting diodes. *Appl. Phys. Lett.* **73**, 3550–3552 (1998).
44. Harvey Scher, M. F. S. a. J. T. B. Time-scale invariance in transport and relaxation. *Phys. Today* **41**, 26 (1991).
45. Cardin, V. *et al.* Recombination dynamics in InGaN/GaN nanowire heterostructures on Si(111). *Nanotechnology* **24**, 045702 (2013).
46. Chang, H. J. *et al.* Direct evidence of nanocluster-induced luminescence in InGaN epilayers. *Appl. Phys. Lett.* **86**, 021911 (2005).
47. Wang, H.-C., Lu, Y.-C., Chen, C.-Y. & Yang, C. C. Carrier capture times of the localized states in an InGaN thin film with indium-rich nanocluster structures. *Appl. Phys. Lett.* **89**, 011906 (2006).
48. Chichibu, S. F. *et al.* Emission mechanisms of bulk GaN and InGaN quantum wells prepared by lateral epitaxial overgrowth. *Appl. Phys. Lett.* **74**, 1460–1462 (1999).
49. Cho, Y.-H. *et al.* “S-shaped” temperature-dependent emission shift and carrier dynamics in InGaN/GaN multiple quantum wells. *Appl. Phys. Lett.* **73**, 1370–1372 (1998).
50. Sun, Y. *et al.* Carrier dynamics of high-efficiency green light emission in graded-indium-content InGaN/GaN quantum wells: An important role of effective carrier transfer. *Appl. Phys. Lett.* **84**, 49–51 (2004).
51. Nguyen, H. P. T. *et al.* Controlling electron overflow in phosphor-free InGaN/GaN nanowire white light-emitting diodes. *Nano Lett.* **12**, 1317–1323 (2012).
52. Nguyen, H. P. T., Djavid, M., Cui, K. & Mi, Z. Temperature-dependent nonradiative recombination processes in GaN-based nanowire white-light-emitting diodes on silicon. *Nanotechnology* **23**, 194012 (2012).
53. Lee, J.-H., Oh, J. T., Kim, Y. C. & Lee, J.-H. Stress reduction and enhanced extraction efficiency of GaN-based LED grown on cone-shape-patterned sapphire. *IEEE Photonics Technol. Lett.* **20**, 1563–1565 (2008).
54. Nguyen, H. P. T., Wang, Q. & Mi, Z. Phosphor-free InGaN/GaN dot-in-a-wire white light-emitting diodes on copper substrates. *J. Electron. Mater.* **43**, 868–872 (2014).
55. Han, S.-H. *et al.* Effect of electron blocking layer on efficiency droop in InGaN/GaN multiple quantum well light-emitting diodes. *Appl. Phys. Lett.* **94**, 231123 (2009).
56. Wang, C. H. *et al.* Hole injection and efficiency droop improvement in InGaN/GaN light-emitting diodes by band-engineered electron blocking layer. *Appl. Phys. Lett.* **97**, 261103 (2010).
57. Verma, J. *et al.* Tunnel-injection GaN quantum dot ultraviolet light-emitting diodes. *Appl. Phys. Lett.* **102**, 041103 (2013).
58. Kozodoy, P., Hansen, M., DenBaars, S. P. & Mishra, U. K. Enhanced Mg doping efficiency in Al_{0.2}Ga_{0.8}N/GaN superlattices. *Appl. Phys. Lett.* **74**, 3681–3683 (1999).
59. Waldron, E. L., Graff, J. W. & Schubert, E. F. Improved mobilities and resistivities in modulation-doped p-type AlGaIn/GaN superlattices. *Appl. Phys. Lett.* **79**, 2737–2739 (2001).

Acknowledgments

This work is being supported by the Natural Sciences and Engineering Research Council of Canada (NSERC). Part of the work was performed in the McGill University Micro Fabrication Facility. Electron microscopy imaging and analysis with the Titan 80–300³ was carried out at the Canadian Centre for Electron Microscopy, a National facility supported by NSERC and McMaster University. The authors wish to thank Prof. Mark Andrews in the Department of Chemistry and Dr. Songrui Zhao in the Department of Electrical and Computer Engineering at McGill University for helping with the time-resolved PL measurements and MBE growth, respectively.

Author contributions

Z.M., I.S. and H.P.T.N. designed the experiment. H.P.T.N. conducted the MBE growth and device fabrication. H.P.T.N., S.M.S. and A.T.C. performed the EL, PL and power measurements. X.L., Q.W. and H.P.T.N. performed TR-PL measurements and analysis. S.Y.W. and G.A.B. performed STEM studies. M.D. carried out the device simulation. Z.M. and H.P.T.N. wrote the manuscript with contributions from other co-authors.

Additional information

Supplementary information accompanies this paper at <http://www.nature.com/scientificreports>

Competing financial interests: The authors declare no competing financial interests.

How to cite this article: Nguyen, H.P.T. *et al.* Engineering the Carrier Dynamics of InGaN Nanowire White Light-Emitting Diodes by Distributed p-AlGaIn Electron Blocking Layers. *Sci. Rep.* **5**, 7744; DOI:10.1038/srep07744 (2015).



This work is licensed under a Creative Commons Attribution-NonCommercial-NoDerivs 4.0 International License. The images or other third party material in this article are included in the article's Creative Commons license, unless indicated otherwise in the credit line; if the material is not included under the Creative Commons license, users will need to obtain permission from the license holder in order to reproduce the material. To view a copy of this license, visit <http://creativecommons.org/licenses/by-nc-nd/4.0/>